Available online at www.sciencedirect.com

SciVerse ScienceDirect

Proceedings of the Combustion Institute 34 (2013) 3231–3238

Proceedings of the Combustion Institute

www.elsevier.com/locate/proci

DNS of EGR-type turbulent flame in MILD condition

Y. Minamoto *, T.D. Dunstan, N. Swaminathan, R.S. Cant

Department of Engineering, University of Cambridge, Trumpington Street, Cambridge CB2 1PZ, UK

Available online 18 September 2012

Abstract

Three-dimensional direct numerical simulation (DNS) of exhaust gas recirculation (EGR)-type turbulent combustion operated in moderate and intense low-oxygen dilution (MILD) condition has been carried out to study the flame structure and flame interaction. In order to achieve adequate EGR-type initial/inlet mixture fields, partially premixed mixture fields which are correlated with the turbulence are carefully preprocessed. The chemical kinetics is modelled using a skeletal mechanism for methane–air combustion. The results suggest that the flame fronts have thin flame structure and the direct link between the mean reaction rate and scalar dissipation rate remains valid in the EGR-type combustion with MILD condition. However, the commonly used canonical flamelet is not fully representative for MILD combustion. During the flame–flame interactions, the heat release rate increases higher than the maximum laminar flame value, while the gradient of progress variable becomes smaller than laminar value. It is also proposed that the reaction rate and the scalar gradient can be used as a marker for the flame interaction.

Keywords: Direct numerical simulation (DNS); Exhaust gas recirculation (EGR); Moderate and intense low-oxygen dilution (MILD); Flameless combustion; Turbulent premixed flame

1. Introduction

Practical combustion systems are continuously required to be more efficient and more environmentally friendly. In conventional combustion techniques, preheating the unburnt mixture using exhaust gases is one way to improve thermal efficiency of the system. However, preheating also increases the flame temperature, resulting in an increase of thermal NO formation. Therefore it is not possible to achieve both objectives using conventional combustion techniques.

The MILD combustion or "flameless" combustion is characterized by highly preheated mixtures and low temperature rise due to combustion [1–4], in which (1) reactants are diluted with large amount of burnt gases so that the maximum temperature rise, ΔT, is low compared to the autoignition temperature, T_{ign}, for the given fuel and (2) reactants are significantly preheated, higher than T_{ign}. A rigorous definition of MILD regime is $T_r > T_{ign}$ and $\Delta T = T_p - T_r < T_{ign}$ [4], where T_r is the reactant temperature and T_p is the product temperature, and is shown in Fig. 1. Here, the autoignition temperature is about 1100 K for CH_4–air mixture (equivalence ratio, $\phi = 0.8$), which is calculated using a well stirred reactor (WSR) configuration with a residence time of 1 s. This definition of MILD combustion is based on WSR theory and is therefore easily applied to premixed combustion, whereas this is not straightforward for non-premixed systems.

In MILD conditions, the flame temperature is very low compared to conventional flames due to the intense dilution even with the highly

* Corresponding author. Fax: +44 1223 339906.
E-mail address: ym270@cam.ac.uk (Y. Minamoto).

1540-7489/$ - see front matter © 2012 Published by Elsevier Inc. on behalf of The Combustion Institute.
http://dx.doi.org/10.1016/j.proci.2012.06.041

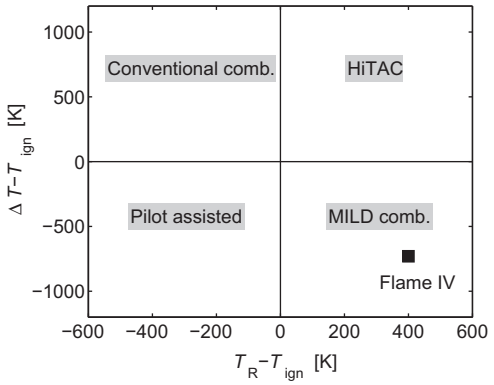

Fig. 1. Combustion-type diagram [4] showing the condition of DNS flame.

preheated unburnt mixture. For instance, Flame IV shown in Fig. 1 has a preheat temperature of 1500 K, while its flame temperature is about 1860 K. Earlier study [1] notes that a sufficient residence time for thermal NO formation is some seconds at around 1900 K and a few milliseconds at around 2300 K, which clearly suggests that the MILD combustion has possibilities for significant NO_x reduction. Therefore, by using MILD technique, it is possible to avoid adverse effect of preheating on flame temperature and reduction of NO_x emissions is no longer limited by the enhancement of thermal efficiency.

The uniformity of temperature due to the high rate of recirculation also helps to reduce combustion instabilities [1,2]. A schematic illustration of combustion with EGR is shown in Fig. 2. In a combustor employing the MILD and EGR techniques, a portion of exhaust gas is recirculated into the mixing chamber (denoted as 'a' in Fig. 2, which will be explained in Section 2.2 later) in order to mix with fresh reactants and exchange the exhaust heat [5]. The exhaust and fresh gases may be partially premixed before combustion occurs in the combustion chamber (denoted as 'b' in Fig. 2), since the mixing time is not long enough to achieve perfect mixing in practice.

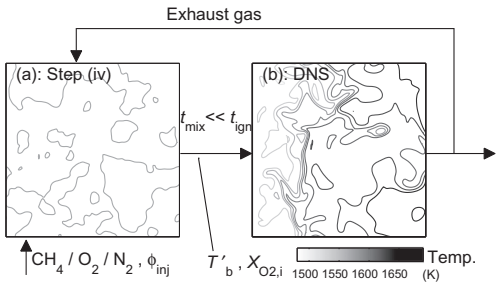

Fig. 2. Schematic illustration of EGR combustor.

Therefore, combustion that takes place in such systems is considered to be different from the traditional turbulent flames: exhaust gas pockets of products and radicals, which are not well mixed before combustion, can lead to additional complexities such as flame–flame interactions.

Several studies have been carried out to further our understanding of MILD combustion [5–12]. From an experimental point of view, no flame front is visible in direct photographs of MILD combustion [6,9,12]. Plessing et al. [5] uses laser diagnostics to compare the instantaneous OH-PLIF and Rayleigh thermometry results between conventional and MILD combustion. In the MILD case, the flame front seems distributed from the temperature field images, while the variation of OH-PLIF suggests presence of flame fronts, although the intensity of OH-PLIF is low compared to the conventional flame. By comparison, OH-PLIF and temperature show similar variation in conventional combustion conditions. Özdemir and Peters [9] also show consistent results from comparison between temperature and OH-PLIF fields. Conventional numerical approaches have also been applied to MILD flames [7,8,10,11] using either flamelet or eddy-dissipation based methods in a Reynolds averaged Navier–Stokes (RANS) context. In most RANS studies, the mean velocity and temperature fields show a consistent trend with the experimental data obtained by laser measurements. However, the predicted peak temperature tends to differ from the experimental results in the range of about 100–600 K, especially when the oxygen concentration is low [11]. It is also shown by Aminian et al. [7] that the prediction of minor species such as OH and CO is sensitive to the temperature fluctuation in RANS.

Given the environmentally-friendly nature of this combustion mode, it is very useful to pose the question: what is the flame front structure in MILD combustion? We believe that finding an answer to this question would help to construct a modelling framework for MILD combustion. Specifically, we like to ask whether flamelet assumptions are valid or whether the flame front is still flamelet like in MILD combustion conditions: from a direct photograph and temperature measurements shown in [5,6,9], the flamelet assumption does not seem to be valid; whereas several numerical studies [8,10] using flamelet models show comparable results with experiments across a range of conditions.

In this study, a three-dimensional DNS of CH_4–air partially premixed flame under MILD condition is carried out using a skeletal mechanism [13]. The flame is analysed from several view points to answer the questions posed above. The DNS detail is discussed in Section 2, the results are presented in Section 3 and the conclusions are drawn in Section 4.

2. DNS of EGR-type combustion

2.1. Configuration and numerical implementation

The numerical code used in this study is SENGA2, an updated version of SENGA [14]. Compressible transport equations are solved on a uniform grid for mass, momentum, total internal energy, and the mass fraction of $N-1$ chemical species using temperature dependent transport properties. Here, a skeletal mechanism [13] comprising $N=16$ species is used. Spatial derivatives are obtained using a tenth order central difference scheme which gradually reduces to a fourth order central difference scheme near boundaries and fourth order one-sided differencing on boundaries. Time integration is achieved using a third order Runge–Kutta scheme.

Figure 3(a) shows the numerical configuration and coordinates. The domain is cubic with a non-reflecting outflow employing Navier–Stokes characteristic boundary conditions (NSCBC) [15] on the down stream (x-direction) face, and periodic conditions in the y and z-directions. A mixture of exhaust gas and fresh premixed gas is fed from the left boundary in the x-direction at an average velocity of U_{in}. The mass fraction of partially premixed mixture, Y_i, and turbulent velocity, $\boldsymbol{u}$, at the inlet ($x=0$) are specified as:

$$\boldsymbol{u}(x=0,y,z,t)=\hat{\boldsymbol{u}}(\underline{x}(t),y,z), \tag{1}$$

$$Y_i(x=0,y,z,t)=\widehat{Y}_i(\underline{x}(t),y,z), \tag{2}$$

where $\hat{\boldsymbol{u}}$ and $\widehat{Y}_i$ correspond to the velocity and partially premixed scalar fields obtained during the preprocessing stage explained in Section 2.2. The x-location of the scanning plane at time t, denoted by $\underline{x}(t)$, moves with velocity U_{in} through pre-computed homogeneous isotropic turbulence and scalar fields, and $\hat{\boldsymbol{u}}$ and $\widehat{Y}_i$ are obtained by interpolating values from the pre-computed domain onto the scanning plane.

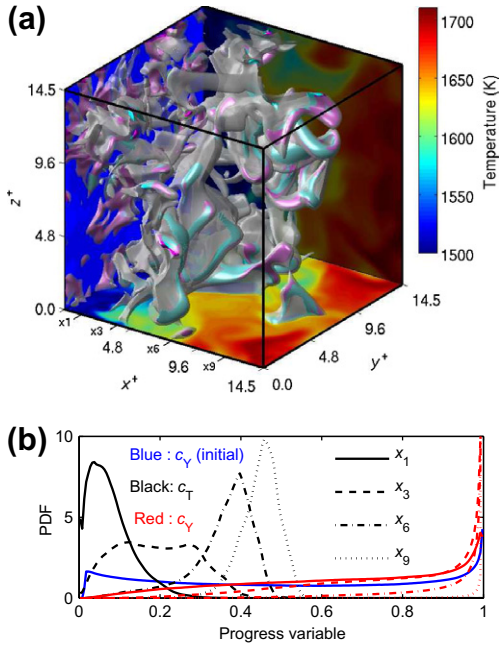

Fig. 3. (a) Iso-surfaces of the reaction rate and x–y, y–z and z–x planes of temperature field. The grey, transparent iso-surfaces correspond to $\omega^{+}_{c_T}=0.7$ and coloured iso-surfaces are $\omega^{+}_{c_T}=1.05$, in which interacting and non-interacting local flame fronts are respectively denoted by purple and light blue colours. (b) PDF of progress variable at x_1, x_3, x_6, x_9 locations. Blue line: $p(c_Y)$ (initial and inlet fields), black lines: $p(c_T)$ and red lines: $p(c_Y)$. (For interpretation of the references to color in this figure legend, the reader is referred to the web version of this article.)

2.2. Preprocessing of scalar and velocity fields for initial and inflow conditions

DNS of a complete EGR combustion system is not yet feasible because of heavy computational cost. Therefore, the combustion phase (b in Fig. 2) is simulated in the present study, and the mixing phase (a in Fig. 2) is taken into account while generating the initial and inflow fields. The mixture used in this DNS is partially premixed between fresh reactants and the exhaust gases, which is assumed as the inlet mixture for the EGR-type combustion. The steps described below are followed to achieve the desired fields of $\hat{\boldsymbol{u}}$ and $\widehat{Y}_i$:

(i) The turbulence field is generated in a preliminary DNS of freely decaying, homogeneous isotropic turbulence in a periodic domain using the initial turbulence obtained as in [16], and the simulation is continued until the turbulence is fully developed.

(ii) A one-dimensional laminar flame is simulated in a desired MILD condition. In the 1D simulation, the unburnt mixture is diluted with H_2O and CO_2 in such way that the molar proportion of H_2O and CO_2 becomes 2:1 (which is the case for complete combustion), and the molar concentration of O_2 matches the desired dilution level.

(iii) A turbulent scalar field is obtained using scalar-energy spectrum function as in [17]. This field is taken as an initial progress variable, c_Y field with values between 0 and 1. Here, $c_Y=1-Y_f/Y_{f,r}$, where Y_f denotes the fuel mass fraction and the subscript, r, denotes values of reactant mixture. In order to construct a mass fraction field from this c_Y field, the 1D flame result obtained in Step (ii) is used. The mass fraction of each species is tabulated relative to the progress variable using the 1D flame result, and the

temperature is set to a constant value T'_b, to be specified later. This scalar field is partially premixed between reactants and products, and the scalar fluctuations do not yet have any correlation with the turbulence obtained in Step (i).

(iv) These scalar and turbulence fields are then allowed to evolve in a periodic domain to mimic the EGR-mixing without reaction. The duration of this mixing DNS is about one large eddy timescale, l_0/u', which is much shorter than the autoignition delay time, where l_0 and u' are respectively the integral length scale and the root-mean-square (rms) of fluctuation of the turbulence obtained in Step (i). During this procedure, the scalar fields develop correlations with the turbulence field. Temperature is also allowed to evolve from a uniform value, T'_b in this step resulting in the maximum temperature fluctuation of about 2.2% of the mean value. The mixture fraction also has variations within a range of about 1.9% of the mean value, which is approximately 0.052 giving $\phi = 0.94$. Here, the mixture fraction is calculated using the definition proposed in [18].

The velocity and scalar fields obtained in the above steps are used as the initial and inlet conditions (a in Fig. 2) in the combustion DNS. The probability density function (PDF) of c_Y in the initial field (after the above preprocessing) is shown in Fig. 3(b) (blue line). Although following step (iii), the progress variable field has a typical bimodal distribution, with two sharp peaks at $c_Y = 0$ and 1, during step (iv) turbulent mixing and molecular diffusion produces samples with intermediate values, $0 \leqslant c_Y \leqslant 1$, with significant PDFs as shown in Fig. 3(b). The mean and variance of this c_Y field are respectively $\langle c_Y \rangle = 0.51$ and $\langle c''^2_Y \rangle = 0.10$.

2.3. Computational parameters and conditions

The regime of combustion in the present DNS is denoted as Flame IV in Fig. 1. The equivalence ratio of the injected mixture shown in Fig. 2, ϕ_{inj}, is 0.8 and the inlet and initial mixture temperatures are set as $T'_b \sim 1500$ K. This inlet temperature might be too high for practical systems. However this high inlet temperature together with the dilution level used in this study shows that the flame condition is strictly in the MILD regime as one can see in Fig. 1. Moreover, the value used in this study is comparable to that used by Suzukawa et al. [19]. The maximum molar fraction of oxygen in the inlet mixture, $X_{O_2,i}$, which indicates the dilution level, is 0.047, and the averaged oxygen molar fraction, $\langle X_{O_2,i} \rangle$, is 0.035. The maximum flame temperature of the 1D laminar flame used in step (ii) of Section 2.2 is about 1860 K, which yields $\Delta T = 360$ K. The unstrained laminar flame speed, S_L, and thermal thickness, $\delta_{th} = (T_p - T_r)/|\$T|_{max}$, for the mixture are respectively 3.20 m/s and 0.691 mm. The Zeldovich thickness, δ_F, which is defined from the ratio between the thermal diffusivity and laminar flame speed is 0.116 mm. The turbulence field obtained in step (iv) has $u'/S_L = 5.13$ and $l_0/\delta_F = 12.8$, where u' is the turbulence intensity and l_0 is the integral length scale. The turbulent Reynolds numbers based on l_0 and Taylor length scale, λ, are $Re_{l_0} = 93.6$ and $Re_\lambda = 31.7$ respectively. The ratio of integral length scales of the turbulence and scalar fields is about 1.58, and the inlet velocity, $U_{in} = 7.82 S_L$. The Karlovitz number is estimated using $Ka \approx (u'/S_L)^{3/2}(l_0/\delta_L)^{-1/2}$ and the Damköhler number is defined as $Da = (l_0/\delta_F)/(u'/S_L)$. In the present DNS, $Ka = 3.25$ and $Da = 2.49$, which is classified as thin-reaction-zones if one uses the classical regime diagram for turbulent premixed flames [20].

The domain has dimensions $L_x = L_y = L_z = 10.0$ mm $(14.5\delta_{th})$, and is discretized using $512 \times 512 \times 512$ uniform grid points, ensuring at least 20 grid points in δ_{th} (based on the diagonal distance between grid points).

The computational domain for the reacting flow simulation was initialized using the fields constructed in Section 2.2 and the simulation was run for 1.5 flow-through times, which is the mean convection time from the inlet to outflow boundaries, to ensure that the initial transients had left. The simulation was then continued for one additional flow-through time and 80 data sets were collected.

DNS has been conducted on Cray XE6 system and the simulation was distributed over 4096 cores and 256 nodes requiring a wall clock time of about 120 hours.

3. Results and discussion

3.1. DNS results and flame interactions

Figure 3(a) shows iso-surfaces of the reaction rate and x–y, y–z and z–x planes of temperature field. The grey, transparent iso-surfaces of reaction rate correspond to $\omega_c^+ = 0.7$ and coloured iso-surfaces are $\omega_c^+ = 1.05$, in which interacting and non-interacting flame elements are respectively shown as purple and light green colours. The criteria to distinguish interacting and non-interacting flames are explained later in this section. The superscript + denotes appropriate normalization using ρ_r, S_L and δ_{th}, where ρ_r is the reactant mixture density. The reaction rate in Fig. 3(a) is the reaction rate of a temperature-

based progress variable, $c_T = (T - T_r)/(T_p - T_r)$ and so is equivalent to the heat release rate. One can also define the progress variable based on c_Y. Since the simulation involves non-unity Lewis numbers, these two progress variables will be different and so both will used in this study.

The flame shown in Fig. 3(a) has a unique shape compared to the conventional turbulent planar flames [21,22] and the presence of flame interactions is obvious. Due to the preheat temperature, regions of intense reaction rate are located not only in the middle of computational domain but in the upstream and downstream regions as well. The maximum temperature in this instantaneous snap-shot is about 1710 K, while it is about 1860 K for the 1D laminar flame used in the step (iv). This is because in the present DNS, the inlet mixture consists of both the diluted premixed reactants with $X_{O_2,i} = 0.047$ and pockets of their products. Thus the mean oxygen level becomes lower in the DNS than the one-dimensional laminar calculation, leading to lower temperature and the desirable MILD condition. Also, in conventional turbulent flames, the peak value of heat release rate is more or less equal to the value in an unstrained laminar flame ($\omega_c^+ \sim 1$) [21,22]. On the other hand, the spatial extent of local flames having $\omega_c^+ \sim 1$ in the present MILD combustion is sparse compared to conventional turbulent flames [22], as shown in Fig. 3(a). This is caused by the EGR configuration, and is due to the existence of exhaust gas pockets and the partially premixed state of inlet mixture.

Probability density function of the progress variables, c_T (black) and c_Y (red), is shown in Fig. 3(b) for four x-locations: $x_1^+ = 1.25$ ($\tilde{c}_T = 0.078$, $\tilde{c}_Y = 0.653$); $x_3^+ = 3.88$ ($\tilde{c}_T = 0.188$, $\tilde{c}_Y = 0.800$); $x_6^+ = 7.78$ ($\tilde{c}_T = 0.352$, $\tilde{c}_Y = 0.963$); $x_9^+ = 11.7$ ($\tilde{c}_T = 0.447$, $\tilde{c}_Y = 0.998$). Although one can distinguish flame fronts in terms of the reaction rate, as shown in Figs. 3(a) and Fig. 4, the temperature based progress variable field does not have a clear bimodal distribution. Especially, for x_3 location the PDF of c_T indicates that the probability of finding reacting gas is relatively high (about 3–4). This is because the flame thickness based on c_T in the DNS, is sometimes much thicker than δ_{th} in one-dimensional DNS due to the facts that (1) heat conduction towards the exhaust gas pockets from the inlet, which do not generate much heat release and (2) the heat release is distributed among many species, and so is more spread out in space because of differential diffusion compared to the single species Y_{CH_4}. On the other hand, the PDFs of c_Y (red lines) show different distributions compared to those of c_T. In particular, the probability of finding fresh reactants is small for all the locations shown because of the presence of exhaust gas pockets in the inlet mixture, and the mixing and fuel consumption in the upstream region. However, since the probability of finding reacting gas is also small compared to the PDF of c_T, it is observed that c_Y field has larger gradient and so thinner fronts. The comparison of PDF of c_T and c_Y is also consistent with the difference of temperature and OH-PLIF fields measured in past experimental studies [5,9] using EGR-type combustor in which the OH-PLIF shows clear flame fronts while the flame fronts in the temperature field seems distributed. If one uses unity Lewis number in DNS, these difference would not be observed.

Successive snapshots of the reaction rate are shown in Fig. 4(a)–(c) in a x–z plane to study the flame front structure and flame interactions. The y-location for the x–z plane changes with time depending on the fluid velocity in the y-direction at $n^+ = 0$. The inset figures show variations of c_T, its gradient and reaction rate as a function of the flame normal distance, n^+, during a flame interaction process at an arbitrarily chosen location. The normal distance of $n^+ = 0$ at each time corresponds to the circle shown on the reaction rate contour lines. This circle moves in Lagrangian sense with time. It should be noted that the normal distance is calculated using the local ∇c_T.

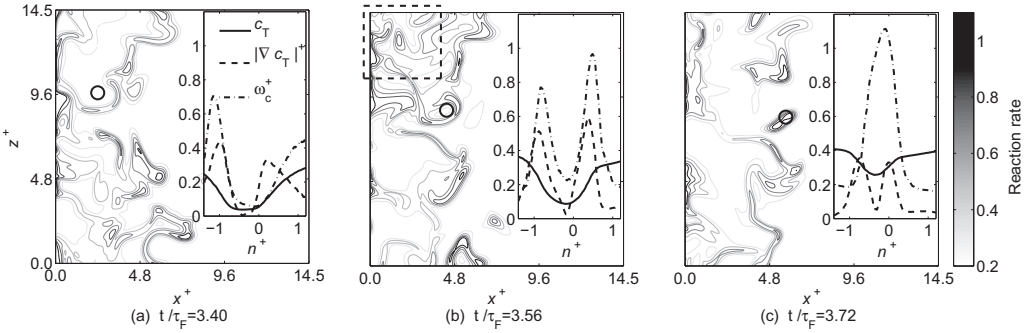

Fig. 4. Two-dimensional slice of reaction rate field. Plots of an arbitrarily chosen flame interaction process as a function of flame normal distance is shown in the insets.

Therefore, the normal direction is not on the x–z plane in general. The duration of time between Fig. 4(a) and 4(c) is about $0.32\tau_F$, where $\tau_F = \delta_{th}/S_L$.

It is generally suggested that there is no flame fronts in MILD conbustion, which is otherwise known as "flameless combustion" [1,4]. In contrast, the present DNS indicates that reactions occur in thin flamelets as shown in Figs. 4(a)–(c). However, as shown in Fig. 4(b), top-left marked with a dotted square, the presence of some interacting flames gives non-flamelet like structure.

The inset in Fig. 4(a) shows that two local flames have a thickness of about δ_{th} in terms of the gradient of progress variable. The flame on the left has a flamelet like structure, since the reaction rate is sharply peaked, while the flame on the right shows a relatively large thickness and smaller gradients of c_T. The inset in Fig. 4(b) shows the same flames as in the inset of Fig. 4(a) after $0.16\tau_F$ and this is considered as the beginning of flame–flame interaction. At this stage of the flame interaction, the reaction rate at around $n^+ = 0$ slightly increases, and both of the flames have a thin flamelet structure with peak values for ω_c^+ of about 0.8 and 1.0. Note that the two flame fronts have intense heat release at this stage, since $\omega_c^+ \sim 1$. The progress variable also increases at $n^+ = 0$, and the gradient of progress variable shows high values at the locations of intense heat release. This is typical of flamelet type combustion as discussed in Section 3.2. The inset in Fig. 4(c) shows that two flames are merged in terms of the reaction rate. The peak value of reaction rate is about 1.1, which is larger than the non-interacting flames shown in Fig. 4(b). On the other hand, the normalized gradient of progress variable, $|\nabla c_T|^+$, at the locations of intense heat release rate ($\omega_c^+ > 1$ for instance) ranges from 0.05 to 0.3, which is very small compared to the non-interacting flames shown in the inset of Fig. 4(b) ($|\nabla c_T|^+ \sim 0.5$–0.6 at the locations of intense heat release rate). Thus it is clear that conventional flamelet type approaches might not be able to describe the flame–flame interaction sufficiently. Although, the maximum value of the normalized reaction rate during the flame interaction is about 1.1 in Fig. 4, values up to about 1.6 (not shown here) were found in the data in interacting flame regions. Also, the locations of instantaneous interacting flames are shown on the iso-surfaces of reaction rate as purple colour in Fig. 3(a). The criteria for flame interaction used here are $\omega_c^+ > 1.0$ and $|\nabla c|^+ < 0.3$. Since the reaction rate of the interacting flame shows non-interacting flame like structure, it is not possible to distinguish interacting flames using only the reaction rate. Although these thresholds are tentatively defined based on Fig. 4(a)–(c), by using these criteria it is possible to distinguish interacting flames from non-interacting flames in order to assess the effect of flame interactions on models in future work.

3.2. Assessment for flamelet approach

It is also our interest to see the relation between the mean reaction rate, $\bar{\omega}_c$, and the mean scalar dissipation rate, $\tilde{\epsilon}_c$, especially to find if flame interactions have a significant effect on this relation in the RANS context. Here the tilde denotes Favre (density-weighted) time average. Under the conditions of high turbulent Reynolds number and Damköhler number together with unity Lewis number, the mean reaction rate is related to the mean scalar dissipation rate as [23]:

$$\bar{\omega}_c = \frac{2}{2C_m - 1}\bar{\rho}\tilde{\epsilon}_c, \tag{3}$$

where C_m is the model parameter defined as:

$$C_m = \int_0^1 c\omega_c P(c)dc \Big/ \int_0^1 \omega_c P(c)dc, \tag{4}$$

and the typical value of C_m is 0.7–0.8 for lean turbulent premixed hydrocarbon flames, where $P(c)$ is the marginal PDF of the progress variable. Eq. (3) is strictly valid when the flame front is thin compared to the Kolmogorov length scale of the turbulence. Under such conditions, the progress variable field has a bimodal distribution. This situation is typically known as flamelet combustion in general. However, this expression for the mean reaction rate is sufficiently accurate even for thin reaction zones regime combustion [24]. In order to study the direct relation between the mean reaction rate and mean scalar dissipation rate, the model parameter, C_m, is calculated from Eq. (3) for both c_T and c_Y and is shown in Fig. 5 as a function of Favre-averaged progress variable. As one observes, C_m has a large variation for c_Y, while it is nearly constant for c_T. This difference is because of the non-unity Lewis number effects. Otherwise these two values for C_m would be close.

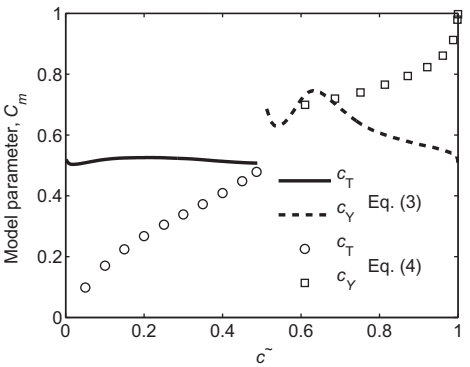

Fig. 5. Model parameter C_m as a function of $\tilde{c}$.

However, these variations of C_m supports the use of Eq. (3) as a possible model for the mean reaction rate in MILD combustion also.

By denoting the volume of interacting flame fronts as V_{int}, obtained using the criterion given in Section 3.1, the ratio V_{int}/V_{tot} is about 36% when the flame front volume, V_{tot}, is obtained using the condition $\omega_c^+ > 1.0$. This ratio drops to about 5% when $\omega_c^+ > 0.7$ is used to obtain V_{tot}. Despite these observations, the relation between the mean reaction rate and the scalar dissipation rate does not show the effect of the flame interactions in a time-averaged sense. Also, as explained in Section 3.1, the PDF of c_T shows that c_T field does not seem to have a bimodal distribution. However, it can be said based on Fig. 5 that Eq. (3) remains sufficiently valid. These results are consistent with the results of laser measurements [5,9] and conclusions of RANS simulations [8,10], in which the predicted fields have consistent trends with experimental results while measured temperature fields show distributed flame fronts (non-bimodal distribution of c_T).

If one uses Eq. (4) to obtain C_m then its value would strongly depend on the PDF for the standard structure of the flamelet function $\omega_c(c)$ [23]. The C_m calculated using the PDFs in Fig. 3(b) and $\omega_c(c)$ obtained from the unstrained planar flamelets is shown in Fig. 5, which consists the result in [23]. The difference in C_m values obtained using Eqs. (3) and (4) is because the canonical flamelet does not include the effects of flame interactions and the presence of exhaust gas pockets in the reactants. This suggests that an appropriate canonical flamelet needs to be identified although the flamelet type modelling is a good approximation for the MILD combustion condition discussed here.

4. Conclusions

Three-dimensional DNS of EGR-type turbulent flame has been conducted under a MILD condition using a skeletal mechanism with non-unity Lewis numbers and following conclusions are obtained.

- The presence of exhaust gas pockets yields a non-bimodal PDF for c_T and it does not influence the bimodal behaviour of c_Y.
- The reaction are observed to occur in thin regions although occasional flame interaction gives a distributed structure.
- During a flame–flame interaction, the local reaction rate becomes larger than the unstrained laminar peak value while the gradient of progress variable at the location of intense reaction rate becomes very small. It is also proposed that these two quantities can be used as a marker for the flame interactions.
- The direct relation between the mean reaction rate and scalar dissipation rate is observed to be sufficiently valid even in EGR-type combustion under MILD condition, although the classical one-dimensional unstrained flame might not be a fully representative canonical flamelet. The construction of a suitable flamelet is of future interest.

Acknowledgements

Y. M. acknowledges the financial support of Nippon Keidanren. EPSRC support is acknowledged by T.D.D. and N.S. This work made use of the facilities of HECToR, the UK's national high-performance computing service, which is provided by UoE HPCx Ltd at the University of Edinburgh, Cray Inc and NAG Ltd, and funded by the Office of Science and Technology through EPSRC's High End Computing Programme.

References

[1] J.A. Wünning, J.G. Wünning, *Prog. Energy Combust. Sci.* 23 (1997) 81–94.
[2] M. Katsuki, T. Hasegawa, *Proc. Combust. Inst.* (1998) 3135–3146.
[3] A. Milani, A. Saponaro, *IFRF Combust. J.* (2001) 200101.
[4] A. Cavaliere, M. de Joannon, *Prog. Energy Combust. Sci.* 30 (2004) 329–366.
[5] T. Plessing, N. Peters, J.G. Wünning, *Proc. Combust. Inst.* (1998) 3197–3204.
[6] M. de Joannon, A. Saponaro, A. Cavaliere, *Proc. Combust. Inst.* 28 (2000) 1639–1646.
[7] J. Aminian, C. Galletti, S. Shahhosseini, L. Tognotti, *Appl. Thermal Eng.* 31 (2011) 3287–3300.
[8] P.J. Coelho, N. Peters, *Combust. Flame* 124 (2001) 503–518.
[9] I.B. Özdemir, N. Peters, *Exp. Fluids* 30 (2001) 683–695.
[10] B.B. Dally, E. Riesmeier, N. Peters, *Combust. Flame* 137 (2004) 418–431.
[11] F.C. Christo, B.B. Dally, *Combust. Flame* 142 (2005) 117–129.
[12] N. Krishnamurthy, P.J. Paul, W. Blasiak, *Proc. Combust. Inst.* 32 (2009) 3139–3146.
[13] M.D. Smooke, in: M.D. Smooke (Ed.), *Lecture Notes in Physics: Reduced Kinetic Mechanisms and Asymptotic Approximations for Methane-Air Flames*, vol. 384, Springer-Verlag, New York, 1991, pp. 1–28.
[14] K. Jenkins, R. Cant, in: Knight, Sakell (Eds.), *Proc. Second AFOSR Conf. on DNS and LES, Rutgers University*, Kluwer Academic Publishers, 1999, pp. 192–202.
[15] T. Poinsot, S. Lele, *J. Comput. Phys.* 101 (1992) 104–129.
[16] R.S. Rogallo, *NASA TM* (1981) 81315.
[17] V. Eswaran, S.B. Pope, *Phys. Fluids* 31 (1987) 506–520.

[18] R.W. Bilger, S.H. Stårner, R.J. Kee, *Combust. Flame* 80 (1990) 135–149.
[19] Y. Suzukawa, S. Sugiyama, Y. Hino, M. Ishioka, I. Mori, *Energy Convers. Mgmt* 38 (1997) 1061–1071.
[20] N. Peters, *Turbulent Combustion*, Cambridge University Press, Cambridge, UK, 2000.
[21] M. Baum, T.J. Poinsot, D.C. Haworth, N. Darabiha, *J. Fluid Mech.* 281 (1994) 1–32.
[22] Y. Shim, S. Tanaka, M. Tanahashi, T. Miyauchi, *Proc. Combust. Inst.* 33 (2011) 1455–1462.
[23] K.N.C. Bray, *Proc. Combust. Inst.* 17 (1979) 223–233.
[24] N. Chakraborty, N. Swaminathan, *Flow Turbulence Combust* (2010), 10.1007/s10494-010-9305-.